Prediction of enantioselectivity by monitoring reaction intermediates

Roelant Hilgers,[a,b] Sin Yong Teng,[a] Anamarija Briš,[a] Aleksandr Y. Pereverzev,[a] Paul White, [a] Jeroen J. Jansen[a] and Jana Roithová[a]*

[a] Institute for Molecules and Materials, Radboud University, Heyendaalseweg 135, 6525 AJ Nijmegen, The Netherlands

[b] Present address: Wageningen University & Research, Droevendaalsesteeg 4, 6708 PB Wageningen, The Netherlands

E-mail: j.roithova@science.ru.nl

Abstract

Enantioselective reactions are at the core of chemical synthesis. Their development mostly relies on prior knowledge, laborious product analysis and post-rationalization by theoretical methods. Here, we introduce a simple and fast method to determine enantioselectivities based on mass spectrometry. The method is based on ion mobility separation of diastereomeric intermediates, formed from a chiral catalyst and prochiral reactants, and delayed reactant labeling experiments to link the mass spectra with the reaction kinetics in solution. The data provide rate constants along the reaction paths of the individual diastereomeric intermediates, revealing the origins of enantioselectivity. Using the derived kinetics, the enantioselectivity of the overall reaction can be predicted. Hence, this method can offer a rapid discovery and optimization of enantioselective reactions in the future. We illustrate the method for the addition of cyclopentadiene (CP) to an α,β-unsaturated aldehyde catalyzed by a diarylprolinol silyl ether.

Introduction

Asymmetric catalysis is of major importance in many fields of chemistry.[1-5] For decades, enzymes and transition-metal complexes have been employed as asymmetric catalysts.[4,6-10] In addition, in the past years, organocatalysts such as chiral secondary amines[1,11-14] became important, culminating with the Nobel Prize awarded to MacMillan and List in 2021.[15-17] Nowadays, the development of new enantioselective reactions relies on the optimization of reaction conditions and catalysts, which is typically done by analyzing the yields and enantioselectivities of many parallel reactions. This approach is laborious and requires relatively large amounts of chemicals.[11,12,18-20] Here, we propose a quicker, simpler and more economical approach to analyze enantioselectivity of a reaction based on ion mobility spectrometry-mass spectrometry.

The efficient development of new reactions requires mechanistic understanding.[21,22] In enantioselective reactions it is particularly important to understand how the two (or more) diastereomeric intermediates react, via competing pathways, to one of the two product enantiomers. However, experimental tracking of such competing reaction paths is challenging, because the intermediates are low-abundant. Consequently, scientists mostly use *ex situ* analysis of isolated 'intermediates'[23-27] and post-rationalization by computational chemistry. Such approach, however, does not necessarily reveal all reaction details and, even worse, can be driven by confirmation bias. To overcome this, the reaction kinetics of diastereomeric intermediates should be monitored *in situ*.[28]

A well-established technique for the investigation of reaction intermediates is electrospray ionization-mass spectrometry (ESI-MS).[29-33] The advantage of ESI-MS over other popular analytical techniques consists in a parallel monitoring of analytes according to their specific mass-to-charge ratios (*m/z*) and in the unprecedented sensitivity.[34,35] With the advent of ion mobility (IM)-mass spectrometry, also isomers, including diastereomers, can be separately detected.[36-39] Thus, ESI-IM-MS opens a way to monitor diastereomeric reaction intermediates in enantioselective reactions. In this paper, we demonstrate the power of the ESI-IM-MS approach for tracking diastereomeric reaction pathways of the asymmetric addition of cyclopentadiene (CP) to *p*-methoxycinnamaldehyde catalyzed by a diaryl prolinol silyl ether (Fig. 1).

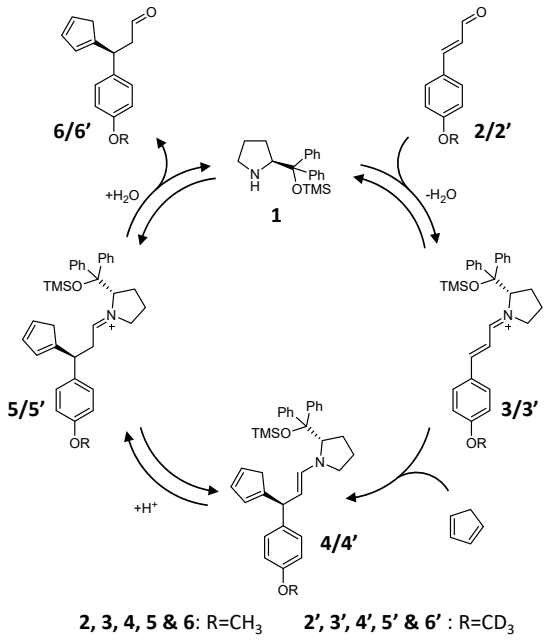

Fig. 1 Suggested reaction mechanism for the enantioselective addition of cyclopentadiene (CP) to an α,β-unsaturated aldehyde, based on Gotoh et al.[40] Intermediates **3**, **4** and **5** and product **6** are formed as multiple isomers, but we show only the dominant isomeric structure here. In the delayed reactant labelling experiments (vide infra), we track kinetics of the reaction steps by adding D_3-labelled reactant (**2'**) with a reaction time delay of 10 min.

Results & Discussion

Detection and characterization of intermediates

The ESI-MS spectrum of the reaction mixture (Fig. 2a) shows all expected reaction components: protonated catalyst **1** (*m/z* 326), sodiated aldehyde **2** (*m/z* 185), the primary iminium intermediate **3** (*m/z* 470) as well as the secondary iminium intermediate **5** (*m/z* 536). The detected iminium ions **5** may correspond to the iminium ions present in solution, but they can be also formed by protonation of enamines **4** upon ESI. In addition, we have detected ions with *m/z* 236, corresponding to the elimination of TMSOH from the protonated catalyst, which presumably occurs during the ionization process (see Supplementary Information for explanation).

Separation of the detected ions based on their ion mobilities reveals three isomeric forms of both the primary and secondary iminium intermediates (**3a**-**3c** and **5a**-**5c** in Fig. 2). In the reaction studied here, the formation of the iminium ions **3** has been shown to be the rate-determining step;[40] therefore, the **3a** : **3b** : **3c** ratios could directly serve as an initial estimate for the enantioselectivity of the reaction. Since we proved, by comparison with an NMR analysis (see Fig. S2), that the isomers of **3** have equal ionization efficiencies, the isomer ratios could directly be obtained from the relative peak areas in the mobilogram.

Integration resulted in a **3a** : **3b** : **3c** ratio of 0.3% : 9.5% : 90.2% (Fig 2c). A control preparative experiment run under the same reaction conditions resulted in 88.5 % of the major product enantiomer (*R*) and 11.5 % of the minor product enantiomer (*S*), which is indeed in a good agreement with the ratio of the two main isomers of **3** (see SI for the details). However, to make the prediction quantitative and applicable to other types of reactions,[41] we must know the kinetics along the entire reaction pathways. In this case, we must determine which isomer of **3** reacts to which isomer of **4** and **5** and what is the kinetics along these competing reaction paths. To this end, we first characterized the individual intermediate isomers in more detail.

Characterization of the isomers of intermediate 3

The condensation of secondary amine catalysts with α,β-unsaturated aldehydes has been reported to result in iminium isomers with *trans* and *cis* C=N bonds, the former typically being the major isomer.[23,24] To verify that the two most abundant isomers of **3** (i.e. **3c** and **3b**) indeed correspond to the *trans* and the *cis* isomers, we performed NMR experiments with an equimolar mixture of catalyst **1** and compound **2** (omitting CP). From the spectra, two iminium isomers could be distinguished with a ratio (~0.05:1) similar to that of **3b** and **3c** in the mobilograms (see Fig. S2). Based on the unique NOESY correlations of these isomers, we confirmed that **3b** and **3c** correspond to the *cis* and the *trans* isomers, respectively, of the iminium ion **3** (Fig. 2b). We further confirmed the identity of **3b** and **3c** by finding a good agreement between the ratio of their theoretical CCSs and the ratio of their inverse ion mobilities ($1/k_0$), as CCS and $1/k_0$ are linearly correlated (Fig. 2d).[42] Despite multiple NMR and IRPD experiments (see Supplementary Information), the exact structure of the low-abundant isomer **3a** could not be elucidated. Nevertheless, its identity is of low importance for the current study, because the expected amount of product formed via **3a** is negligible (*vide infra*).

Characterization of the isomers of intermediates 4 & 5

The ions of *m/z* 536 could correspond to both, protonated enamines **4** and/or iminium ions **5**. Protonation of the enamines during ESI could occur at the nitrogen atom or at the β-carbon atom. However, the IR photodissociation spectrum of the ions with *m/z* 536 does not show any N-H stretching vibration (no band above 3100 cm^{-1}; see Fig. S3) suggesting that N-protonated enamines do not form. In agreement, DFT calculations indicate that C-protonation is favored by 10-12 kcal mol^{-1} (Table S2). Hence, intermediates **4** and **5** are collectively detected as iminium ions **5** in ESI-MS experiments.

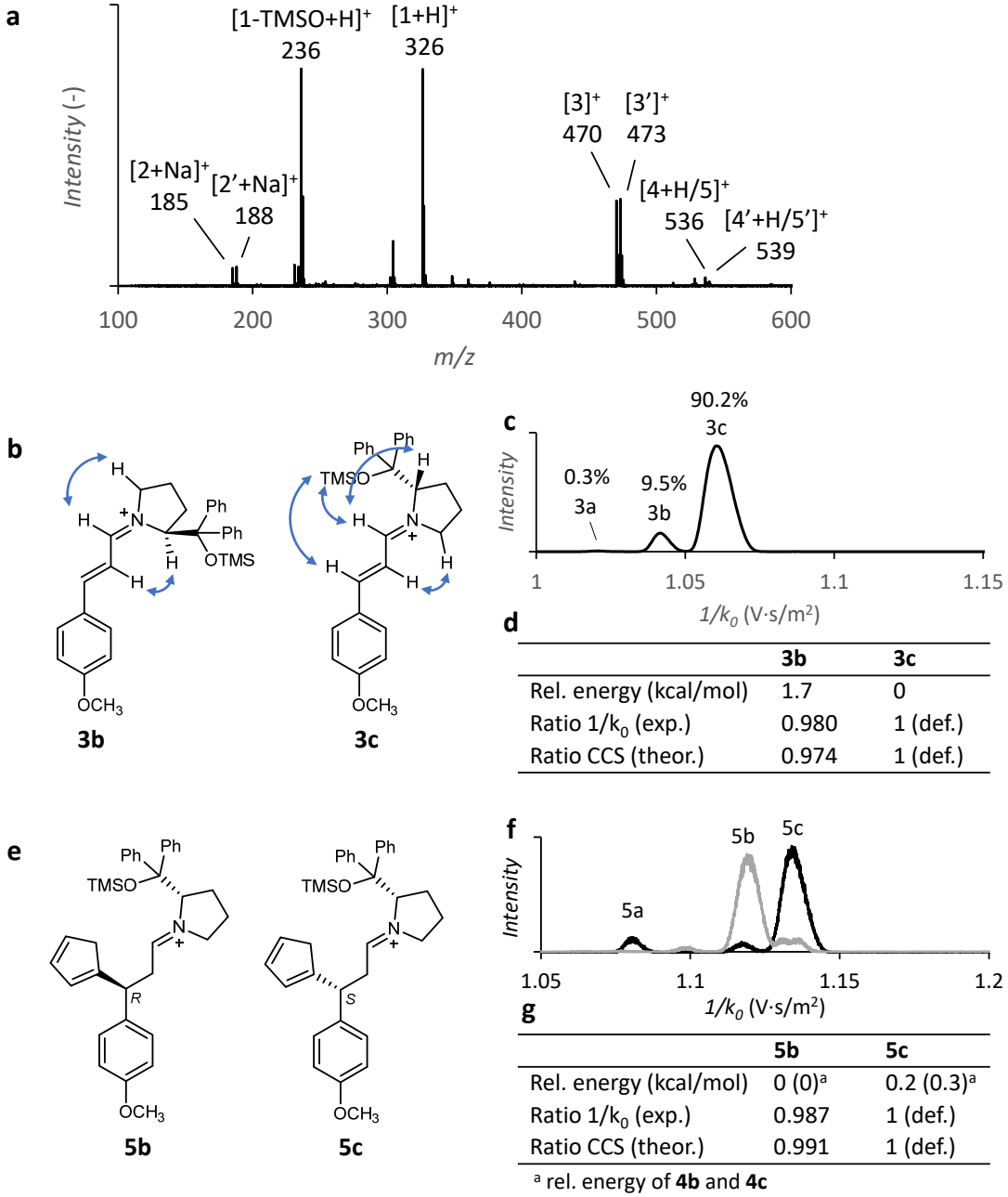

d	3b	3c
Rel. energy (kcal/mol)	1.7	0
Ratio $1/k_0$ (exp.)	0.980	1 (def.)
Ratio CCS (theor.)	0.974	1 (def.)

g	5b	5c
Rel. energy (kcal/mol)	0 (0)[a]	0.2 (0.3)[a]
Ratio $1/k_0$ (exp.)	0.987	1 (def.)
Ratio CCS (theor.)	0.991	1 (def.)

[a] rel. energy of **4b** and **4c**

Fig. 2 a, ESI-MS spectrum of the reaction mixture after 25 min total reaction time. Isotopically labeled reactant **2'** was added after elapsing of 10 min reaction time. **b**, Structure annotations of the of iminium isomers **3b** and **3c**, with diagnostic NOESY correlations shown as blue arrows. Detailed NMR results (1H NMR, TOCSY and NOESY) can be found in the Supplementary Information. **c**, Mobilogram of the ions with *m/z* 470, the numbers refer to the peak areas. **d**, Relative energies and collisional cross sections of **3b** and **3c**. **e**, Structure annotations of ions **5b** and **5c**. **f**, Mobilograms of the ions with *m/z* 536 generated obtained from the reaction mixture of **1** and **2** (i.e. forward reaction, in black) and from the mixture of **1** and the product isomers **6** (reverse reaction, in gray). Both mobilograms display the ion mobility distribution after approximately 15 min reaction time. **g**, Relative energies and collisional cross sections of **5b** and **5c**; values in brackets refer to the relative energies of neutral enamines **4b** and **4c**.

To find out which isomer of the iminium ions **5** reacts to the major product, we have isolated the isomeric mixture of product **6** after the completion of the reaction and mixed it with catalyst **1** to form the iminium ions **5**. Since product **6** is a mixture of *R* (major) and *S* (minor) enantiomers, the reverse reaction is expected to produce at least two isomers of **5**: a major isomer with the cyclopentadienyl group linked in the *R*-configuration, and a minor isomer with the cyclopentadienyl group linked in the *S*-configuration. The ESI-IM-MS analysis clearly shows that iminium **5b** is the most abundant isomer formed in the reverse reaction, and that **5c** is formed in a lower amount, suggesting that **5b** and **5c** report on the *R* and *S*-isomers of intermediates **4**/**5**, respectively (Fig. 2f in gray). Further evidence for this annotation was provided from the excellent agreement between the ratio of the theoretical CCSs and experimental inverse mobilities of **5b** and **5c** (Fig. 2g). The isomer **5a** was not detected in the reverse reaction. We hypothesize that **4a**/**5a** are formed from **3a**, and correspond to a side product that was removed during the purification of product **6**. The rate of the reverse conjugated addition is almost negligible, because we did not detect iminium intermediates **3** in the reverse reaction (except trace amounts after long reaction times).

The above-described annotations allow us to identify the reaction pathways of the individual isomeric intermediates (Fig. 3). The reactant and the catalyst condensate to mainly form iminium ions **3c** and **3b**, which have C=N bonds in the *trans* and *cis*-configurations, respectively. The bulky catalyst side chain forces the CP to attack from the least sterically hindered side of the iminium intermediate.[23,43] Accordingly, **3c** reacts via **4b** and **5b** to yield the *R*-enantiomer of product **6**, and **3b** reacts via **4c** and **5c** to yield the *S*-enantiomer of **6**. Isomer **3a** probably reacts via **4a**/**5a** to a side product.

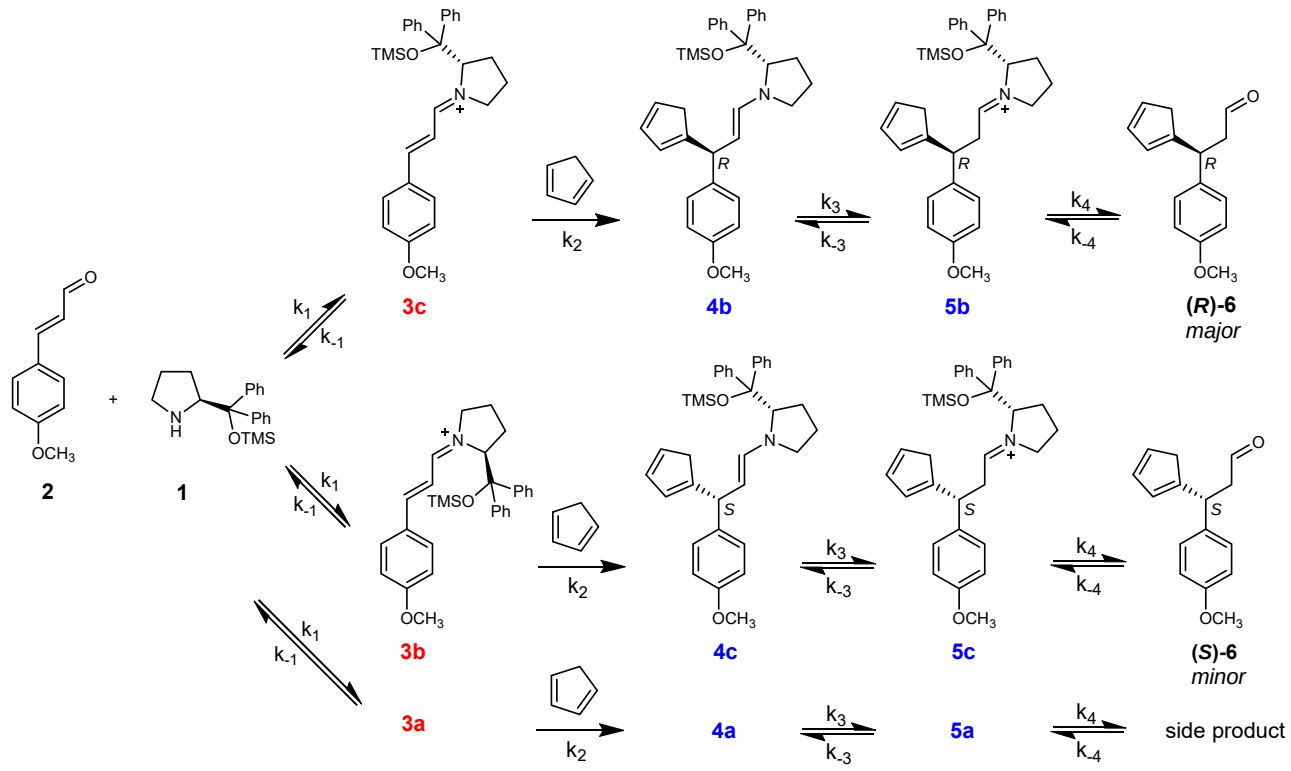

Fig. 3 Proposed reaction pathways based on NMR, IRPD and ESI-IM-MS experiments described in the main text. The exact structures of **3a** and **4a**/**5a** are unknown and are therefore not shown.

Determination of the rate constants for the individual isomeric intermediates

Although the ratio of the primary intermediate abundances (**3c** : **3b**) gives a good estimate for the enantioselectivity in this particular reaction, it cannot be taken as a general rule. The enantioselectivity can be affected by the equilibria involving all the other intermediates along the reaction pathways.[44-47] Hence, for a complete and correct evaluation we need to know the rate constants indicated in Fig. 3 for all competing pathways. To determine these rate constants, we need to monitor the concentration changes of the intermediates in time. In general, the ion intensities in ESI-MS spectra do not necessarily correlate with the concentrations of the analytes in solution.[48] However, we have developed a method to overcome this problem by using so-called delayed reactant labeling (DRL).[49]

The key point of DRL is that one of the reactants is added as a mixture of unlabeled and isotopically labeled molecules and that one of them is added with a certain time delay. The ratio between labeled and unlabeled intermediates is then monitored over time. For intermediates displaying steady-state kinetics, this

ratio reflects the depletion rate of these intermediates.[49] The principle behind DRL and a theoretical outcome of such an experiment are illustrated in Fig. 4, using a simple two-step reaction.

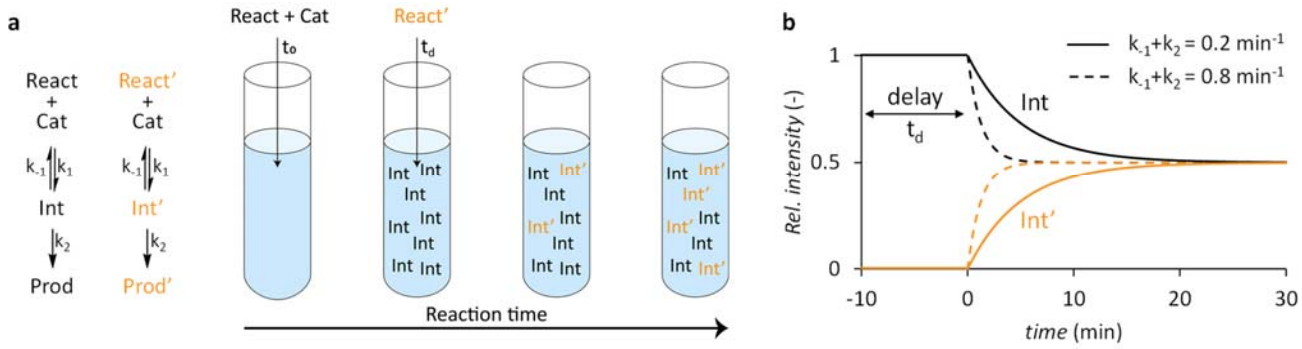

Fig. 4 A schematic example of a delayed reactant labeling (DRL) experiment. In (a) the equations are shown for a simple two-step reaction of the unlabeled (black) and isotopically labeled (yellow) reactant along with a schematic representation of the ratio of labeled/unlabeled intermediates in solution at various stages of the DRL experiment. In (b) a graph is displayed showing theoretical outcomes of a DRL experiment with a time delay of 10 min. Increased values of k_{-1} and k_2 result in a shorter lifetime of the intermediate, and thereby in the increased slopes in the DRL curves. For intermediates displaying steady-state kinetics, depletion rate constants ($k_{-1}+k_2$) can be derived using equation 1 (see the methods section).

To monitor the kinetics of the reaction studied here, we have added D_3-labeled *p*-methoxy-cinnamaldehyde (**2'**) to the reaction mixture with a delay of 10 min. The relative abundances of the isotopically labeled intermediates (**3'** and **5'**) gradually increased over time for all isomers (Fig. 5a and 5b), confirming that they are formed in solution (i.e. not during ESI).[50] All isomers of **3** display steady state kinetics, as demonstrated by i) the rapid establishment of a 1:1 equilibrium of **3** and **3'** (corresponding to the 1:1 concentrations of **2** and **2'**) after addition of **2'** (Fig. 5c-e) and ii) the fact that the TIC-normalized intensities of **3** and **3'** (TIC = total ion current) remain essentially constant after reaching the equilibrium conditions (Fig. 5a). Thus, we derived the degradation rate of all isomers of **3** ($k_{-1} + k_2$) by fitting the DRL curves using equation 1 (see methods section). To determine the individual contributions of k_{-1} and k_2, the experiment was repeated in absence of CP, so that k_2 equals 0. In this experiment, the iminium ions **3** did not reach steady-state concentrations within the experimental time; using the Euler method, k_{-1} was estimated to be approximately 0 (Fig. S5&S6). This indicates that, under the experimental conditions used, the hydrolysis rates (k_{-1}) of **3a-c** are negligible compared to their reaction rates with CP (k_2) (Table 1).

The determination of the rate constants of intermediates **4** and **5** is somewhat more challenging. As there is a lag phase in the formation of **4'** and **5'** (Fig 5c-e), their relative intensities cannot be fitted by using equation 1. Additionally, since enamines **4** are detected as iminium ions **5** in the ESI-MS experiments, it is impossible to record the intensity of intermediates **4** and **5** separately. Nonetheless, by simultaneously fitting the relative ion intensities of **5'** (Fig. 5c-e) and the isomer ratios (Fig. 5f&g), separate rate constants

could be derived for intermediates **4** and **5** (Table 1). In fact, without considering separate kinetics for **4** and **5**, we were unable to obtain a reasonable fit of the experimental data, which indicates that both species are necessary to explain the obtained variations in the concentrations.

From the fitted data of the DRL experiments, several direct insights into the reaction can be obtained. Firstly, k_2 of isomer **3b**, reacting to the minor *S*-product, was found to be higher than that of **3c**, which reacts to the major *R*-product (Table 1). This, obviously, reduces the overall enantiomeric excess (*e.e.*) of the reaction. The faster reaction could be a result of the steric strain in the **3b** intermediate that can be released after the formation of enamine **4b** (see structures and relative energies in Fig. 2). Remarkably, the opposite (*i.e.*, higher k_2 for the major isomer) has often been suggested for similar iminium-catalyzed reactions, to explain the higher *e.e.* as compared to the *trans*/*cis* ratio of the primary iminium intermediates.[15,23] Additionally, notable differences in the kinetics for the different isomers of intermediates **4** and **5** were observed. A relatively rapid 1:1 equilibrium of the labeled/unlabeled intermediates was obtained for intermediates **4b**/**5b** on the favored pathway, whereas no equilibrium was obtained for intermediates **4a**/**5a** and **4c**/**5c**. Accordingly, the experimental TIC-normalized intensity profiles show that isomers **4a**/**5a** and **4c**/**5c** slowly accumulate in solution whereas **4b**/**5b** reach a constant steady-state concentration (Fig. S7). By fitting the data, the individual concentration profiles were obtained for the enamines (**4**) and iminium ions (**5**), which indicate that there is a buildup of iminium ions **5a** and **5c** in solution, whereas **5b** is rapidly hydrolyzed to the product (Fig. S8). Assuming that CP addition is practically irreversible (vide supra) and that the values of k_{-4}·[**6**] are close to zero (at short reaction times, the concentrations of the products are negligible), the large difference in the hydrolysis rate (k_4) between the isomers of **5** has a negligible effect on the overall enantioselectivity. Under these circumstances the *e.e.* is governed by the ratio **3c** : **3b** (*trans*/*cis*) and their reaction rates with CP (k_2). We note that the large difference in the rate of hydrolysis between the isomers of intermediate **5** could only play a small role in the enantioselectivity when reactions are incomplete, depending on the catalyst concentration (Fig S9).

In order to verify that the method is also suitable to explore the effect of the reaction conditions on the kinetics of isomeric intermediates, the DRL experiment was repeated at a lower temperature (25 °C). Qualitatively, the results were similar to those obtained at 45 °C. Yet, as expected, all intermediates displayed slower kinetics (Fig. S11 and Table S4).

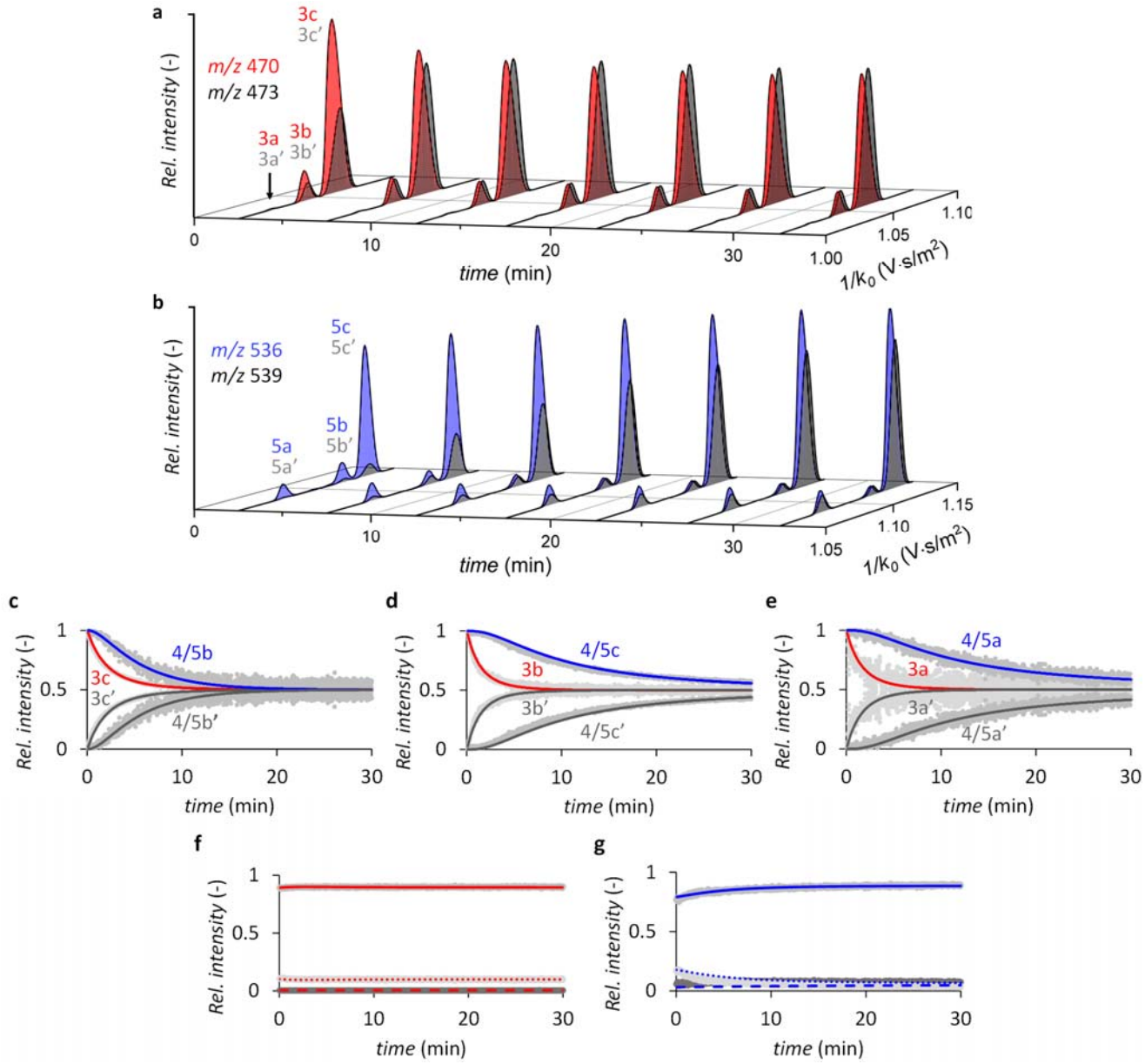

Fig. 5 a&b, TIC-normalized extracted ion mobilograms illustrating the time evolution of individual intermediate isomers for **3** & **3'** (**a**), and **5** & **5'** (**b**). **c-e**, Time evolution of relative ion intensities of labeled vs. unlabeled intermediates in the delayed reactant labeling experiment for the three pathways shown in Fig 3. Experimental relative ion intensities are shown in light gray. Relative intensities obtained by modelling (see Table 1 for rate constants) are shown for ions **3** (red lines) & **3'** (dark gray) and **5** (blue) & **5'** (dark gray). **f&g**, Time evolution of the relative ion intensities of the three isomers of intermediate **3** (**f**) and intermediate **5** (**g**). Both graphs display the experimental relative ion intensity of isomers a (dark grey), isomers b (light gray) and isomers c (gray), as well as the relative ion intensity obtained by modelling: isomer a (dashed line), isomer b (dotted line) and isomer c (solid line). The blue curves were constructed by summing the predicted concentrations of enamine **4** and iminium ion **5**, using a correction factor of 0.025 (a fitting parameter) to account for the lower ionization efficiency of the enamine.

Table 1. Left panel: Rate constants for individual isomeric intermediates obtained by simultaneously fitting the relative intensities of labeled and unlabeled intermediates (Fig. 5c-e) and relative intensities of intermediate isomers (Fig. 5f&g).[a] Right panel: Comparison between the enantiomer ratio of product **6** predicted by the DRL experiment and experimentally determined by chiral HPLC.

Pathway	k_1 M^{-1} min^{-1}	k_{-1} min^{-1}	k_2 min^{-1}	k_{-2} min^{-1}	k_3 min^{-1}	k_{-3} min^{-1}	k_4 min^{-1}	Predicted % of product 6[b,c]	Experimental % of product 6[d]
3c→4/5b	1.50	0.0	0.43	0.025	0.23	0.0	8.0	86.7 ± 1.3 (*R*)	88.5 ± 0.2 (*R*)
3b→4/5c	0.25	0.0	0.64	0.035	0.35	0.0	0.05	13.3 ± 1.3 (*S*)	11.5 ± 0.2 (*S*)
3a→4/5a	0.01	0.0	0.57	0.030	0.30	0.0	0.03	-	-

[a]The values for the duplicate experiment are largely similar and are shown in Table S3. [b]Only the products formed via **3b** and **3c** are considered, since the product formed via **3a** is only formed in negligible amounts (0.6% of the total product) and its identity is unknown. [c]Average and standard deviation were obtained from two independent DRL experiments. [d]Average and standard deviation were obtained from two chiral HPLC runs after derivatization of product **6** (see Supplementary Information).

Prediction of enantioselectivity by ion mobility-mass spectrometry

Combining all individual rate constants of the asymmetric reaction allows us to predict the enantiomer ratio of the final product. By using the rate constants of two duplicate DRL experiments (Table 1 and Table S3), we predicted that 86.7% of the product would occur as the *R*-enantiomer. The products synthetized under the same conditions contained 88.5% of the *R*-enantiomer as determined by chiral HPLC (Table 1). Although, in this case, the accuracy of this prediction is similar to that of the direct estimation from the ratio of iminium ions **3b** : **3c**, we note that the DRL approach is the correct one, and is also applicable to reactions where direct estimation from intermediate isomer ratios cannot be used. We emphasize that the excellent ESI-IM-MS based prediction can be obtained from a ~30 min sub-mg scale experiment. By incorporating predictive machine learning methods, this approach can open a perspective for rapid screening of possible new enantioselective reactions and for optimization of the reaction conditions for enantioselective syntheses. This all without the need to perform multiple parallel syntheses, purifications and HPLC analyses.

Limitations of the current method

As indicated above, the novel DRL method provides quantitative insights into the reaction at a level that is unattainable with other methods. Nevertheless, there are some limitations that deserve to be discussed. For k_1, it is possible to determine a ratio between the values of the three individual pathways. This ratio, after all, determines to a large extent the isomer ratio of intermediate **3** (Fig. 5f). Exact values can, however, not be obtained, as the value of k_1 does not affect the relative intensity evolution of the labeled and unlabeled intermediates. For the same reason, the method is not able to provide values of k_{-4}

related to the formation of the iminium ions from the product. The presented experiments are performed at low conversion yields, therefore we can assume that k_{-4}[Product **6**] is close to 0 and k_{-4} does not play an important role. The k_1 values could be determined from the reaction monitoring of the interaction of **2** with the catalyst by e.g. NMR spectroscopy.

Conclusions

We demonstrated that ion mobility mass spectrometry can be used to predict enantioselectivity in asymmetric reactions. The experiments are quick and can be performed at a (sub-)mg scale. The analysis of the reaction is based on the determining of the rate constants associated with diastereomeric reaction intermediates along the reaction paths using the delayed reactant labeling approach. We illustrated this method for the organocatalytic Michael addition of cyclopentadiene to *p*-methoxycinnamaldehyde. The method is an excellent tool to obtain detailed insights into the mechanisms of asymmetric reactions, and can be used to rapidly screen for optimal reaction conditions, without the need to perform multiple syntheses. In present, the data require a kinetic modelling that can, however, be machine-learned when a database of various reactions is available.

Methods

Reaction mixtures for delayed reactant labeling (DRL) experiments were prepared by mixing stock solutions of (*S*)-(+)-α,α-diphenyl-2-pyrrolidinemethanol trimethylsilyl ether (catalyst **1**), *p*-methoxycinnamaldehyde (compound **2**) and cyclopentadiene in a glass vial to obtain concentrations of 0.167 mM, 3.33 mM and 50 mM, respectively. The reaction mixture was then stirred for 10 min at 45°C, after which *p*-methoxycinnamaldehyde-d_3 (compound **2'**) was added to obtain the final concentrations of 0.1 mM (catalyst **1**), 2 mM (both compounds **2** and **2'**) and 30 mM (cyclopentadiene). Upon addition of compound **2'**, the reaction mixture was infused into the ESI source of the mass spectrometer via a silica capillary by applying a slight overpressure of N_2 (approximately 0.2 bar). Preparation of the reaction mixtures for other experiments is described in the Supplementary Information.

ESI-IM-MS experiments were performed with a Bruker timsTOF instrument in positive ionization mode. The TIMS cell was operated in the ultra mode at a range of 0.93-1.26 V·s/m^2. Detailed settings are described in the Supplementary Information. NMR experiments were conducted on a Bruker Avance III 400 MHz or Bruker Avance III 500 MHz spectrometer. Depending on the solvent of the sample, the residual solvent peak of chloroform (δ_H = 7.26) or formic acid (δ_H = 8.03) was used as the internal reference. IR

photodissociation experiments were performed using helium-tagging method with mass selected ions at 3 K using the ISORI instrument.[51]

For DFT optimizations, the preferred conformers of all isomers were identified by conformational analysis performed with the PM6 method. The lowest energy conformations were further optimized using the B3LYP functional with the D3 dispersion correction and the 6-31G** basis set as implemented in Gaussian 16.[52] For calculations of IR spectra, scaling factors of 0.985 and 0.952 were used in the region below and above 2000 cm^{-1}, respectively. Calculations of CCS of DFT-optimized structures were performed by using collidoscope.[53]

Determination of rate constants by fitting data of DRL experiments

Summed rate constants for the depletion of intermediates **3**/**3'** (i.e. $k_{-1}+k_2$) were obtained by analytical fitting the relative intensity of ion **3'** using equation 1[49]:

$$[\mathbf{3'}]_t = [\mathbf{3'}]_{eq} (1-e^{-(k_{-1}+k_2)\cdot t}) \qquad (1)$$

In which $[\mathbf{3'}]_t$ is the relative concentration of **3'** (with respect to the sum of **3** and **3'**) at time 't' and $[\mathbf{3'}]_{eq}$ is the relative concentration of **3'** after reaching the equilibrium between labeled and unlabeled intermediates. Note that equation 1 is only valid for intermediates displaying steady-state kinetics. To determine separate values for k_{-1} and k_2, a DRL experiment was performed in the absence of CP which showed that k_{-1} is negligible, therefore we used $k_{-1}=0$ in further fitting.

For the determination of all other rate constants, the relative ion intensities and isomer ratios were derived using the Euler numerical integration method (see rate equations S1-S6 and the numerical model in an excel sheet in the Supplementary Information). Fitting of the experimental data was performed by adjusting all rate constants in the model except k_{-1} and k_{-4} which were set to zero and k_2, which was obtained analytically from steady state approximation modelling. Monte-Carlo simulations were performed to validate and to refine the fitting (see the description and the statistical models and the fitting procedure in the Supplementary Information). The Monte-Carlo simulations confirmed the validity of the fits and led to minor changes of the rate constants. The values obtained using the manual fitting are presented in the figures and tables of this article, the Monte-Carlo results are in the Supplementary Information.

Acknowledgements

This work was supported by the NWO grant OCENW.KLEIN.348.

References

1 Han, B. *et al.* Asymmetric organocatalysis: an enabling technology for medicinal chemistry. *Chemical Society Reviews* **50**, 1522-1586 (2021).

2 Zhang, Y.-C., Jiang, F. & Shi, F. Organocatalytic asymmetric synthesis of indole-based chiral heterocycles: strategies, reactions, and outreach. *Accounts of chemical research* **53**, 425-446 (2019).

3 Wang, M. *et al.* Catalytic Asymmetric Synthesis of the anti-COVID-19 Drug Remdesivir. *Angewandte Chemie International Edition* **59**, 20814-20819 (2020).

4 Xue, Y.-P., Cao, C.-H. & Zheng, Y.-G. Enzymatic asymmetric synthesis of chiral amino acids. *Chemical Society Reviews* **47**, 1516-1561 (2018).

5 Hu, P. *et al.* Quaternary-centre-guided synthesis of complex polycyclic terpenes. *Nature* **569**, 703-707 (2019).

6 Thomas, C. M. & Ward, T. R. Artificial metalloenzymes: proteins as hosts for enantioselective catalysis. *Chemical Society Reviews* **34**, 337-346 (2005).

7 Mueller, M. Recent Developments in Enzymatic Asymmetric C-C Bond Formation. *Advanced Synthesis & Catalysis* **354**, 3161-3174 (2012).

8 Katsuki, T. Unique asymmetric catalysis of cis-β metal complexes of salen and its related Schiff-base ligands. *Chemical Society Reviews* **33**, 437-444 (2004).

9 Canali, L. & Sherrington, D. C. Utilisation of homogeneous and supported chiral metal (salen) complexes in asymmetric catalysis. *Chemical Society Reviews* **28**, 85-93 (1999).

10 Chelucci, G. Metal-complexes of optically active amino-and imino-based pyridine ligands in asymmetric catalysis. *Coordination Chemistry Reviews* **257**, 1887-1932 (2013).

11 Marigo, M., Wabnitz, T. C., Fielenbach, D. & Jørgensen, K. A. Enantioselective organocatalyzed α sulfenylation of aldehydes. *Angewandte Chemie* **117**, 804-807 (2005).

12 Hayashi, Y., Gotoh, H., Hayashi, T. & Shoji, M. Diphenylprolinol silyl ethers as efficient organocatalysts for the asymmetric Michael reaction of aldehydes and nitroalkenes. *Angewandte Chemie International Edition* **44**, 4212-4215 (2005).

13 Ahrendt, K. A., Borths, C. J. & MacMillan, D. W. New strategies for organic catalysis: the first highly enantioselective organocatalytic Diels− Alder reaction. *Journal of the American Chemical Society* **122**, 4243-4244 (2000).

14 List, B., Lerner, R. A. & Barbas, C. F. Proline-catalyzed direct asymmetric aldol reactions. *Journal of the American Chemical Society* **122**, 2395-2396 (2000).

15 Donslund, B. S., Johansen, T. K., Poulsen, P. H., Halskov, K. S. & Jørgensen, K. A. The diarylprolinol silyl ethers: ten years after. *Angewandte Chemie International Edition* **54**, 13860-13874 (2015).

16 Aukland, M. H. & List, B. Organocatalysis emerging as a technology. *Pure and Applied Chemistry* **93**, 1371-1381 (2021).

17 Xiang, S.-H. & Tan, B. Advances in asymmetric organocatalysis over the last 10 years. *Nature Communications* **11**, 1-5 (2020).

18 Xiao, J., Zhao, K. & Loh, T.-P. The acid free asymmetric intermolecular α-alkylation of aldehydes in fluorinated alcohols. *Chemical Communications* **48**, 3548-3550 (2012).

19 Gotoh, H., Masui, R., Ogino, H., Shoji, M. & Hayashi, Y. Enantioselective Ene Reaction of Cyclopentadiene and α,β-Enals Catalyzed by a Diphenylprolinol Silyl Ether. *Angewandte Chemie International Edition* **45**, 6853-6856 (2006).

20 Halskov, K. S., Naicker, T., Jensen, M. E. & Jørgensen, K. A. Organocatalytic asymmetric remote aziridination of 2, 4-dienals. *Chemical Communications* **49**, 6382-6384 (2013).

21 Peng, Q. & Paton, R. S. Catalytic control in cyclizations: From computational mechanistic understanding to selectivity prediction. *Accounts of chemical research* **49**, 1042-1051 (2016).
22 Ahn, S., Hong, M., Sundararajan, M., Ess, D. H. & Baik, M.-H. Design and optimization of catalysts based on mechanistic insights derived from quantum chemical reaction modeling. *Chemical reviews* **119**, 6509-6560 (2019).
23 Seebach, D. *et al.* Stereochemical models for discussing additions to α, β-unsaturated aldehydes organocatalyzed by diarylprolinol or imidazolidinone derivatives – is there an '(E)/(Z)-dilemma'? *Helvetica Chimica Acta* **93**, 603-634 (2010).
24 Grošelj, U. *et al.* Structures of the reactive intermediates in organocatalysis with diarylprolinol ethers. *Helvetica Chimica Acta* **92**, 1225-1259 (2009).
25 Halskov, K. S., Donslund, B. S., Paz, B. M. & Jørgensen, K. A. Computational approach to diarylprolinol-silyl ethers in aminocatalysis. *Accounts of chemical research* **49**, 974-986 (2016).
26 Diner, P., Kjaersgaard, A., Lie, M. A. & Jørgensen, K. A. On the origin of the stereoselectivity in organocatalysed reactions with trimethylsilyl-protected diarylprolinol. *Chemistry–A European Journal* **14**, 122-127 (2008).
27 Schmid, M. B., Zeitler, K. & Gschwind, R. M. Distinct conformational preferences of prolinol and prolinol ether enamines in solution revealed by NMR. *Chemical Science* **2**, 1793-1803 (2011).
28 Blackmond, D. G. Kinetic profiling of catalytic organic reactions as a mechanistic tool. *Journal of the American Chemical Society* **137**, 10852-10866 (2015).
29 Eberlin, M. N. Electrospray ionization mass spectrometry: a major tool to investigate reaction mechanisms in both solution and the gas phase. *European Journal of Mass Spectrometry* **13**, 19-28 (2007).
30 Schröder, D. Applications of electrospray ionization mass spectrometry in mechanistic studies and catalysis research. *Accounts of chemical research* **45**, 1521-1532 (2012).
31 Mehara, J. & Roithová, J. Identifying reactive intermediates by mass spectrometry. *Chemical Science* **11**, 11960-11972 (2020).
32 Chen, P. Electrospray ionization tandem mass spectrometry in high-throughput screening of homogeneous catalysts. *Angewandte Chemie International Edition* **42**, 2832-2847 (2003).
33 O'Hair, R. A. Mass spectrometry based studies of gas phase metal catalyzed reactions. *International Journal of Mass Spectrometry* **377**, 121-129 (2015).
34 Belov, M. E., Gorshkov, M. V., Udseth, H. R., Anderson, G. A. & Smith, R. D. Zeptomole-sensitivity electrospray ionization− Fourier transform ion cyclotron resonance mass spectrometry of proteins. *Analytical chemistry* **72**, 2271-2279 (2000).
35 Pan, Z. & Raftery, D. Comparing and combining NMR spectroscopy and mass spectrometry in metabolomics. *Analytical and bioanalytical chemistry* **387**, 525-527 (2007).
36 Lanucara, F., Holman, S. W., Gray, C. J. & Eyers, C. E. The power of ion mobility-mass spectrometry for structural characterization and the study of conformational dynamics. *Nature chemistry* **6**, 281-294 (2014).
37 Greisch, J.-F. *et al.* Detection of intermediates in dual gold catalysis using high-resolution ion mobility mass spectrometry. *Organometallics* **37**, 1493-1500 (2018).
38 Zhang, J.-T., Wang, H.-Y., Zhang, X., Zhang, F. & Guo, Y.-L. Study of short-lived and early reaction intermediates in organocatalytic asymmetric amination reactions by ion-mobility mass spectrometry. *Catalysis Science & Technology* **6**, 6637-6643 (2016).
39 Révész, Á., Schröder, D., Rokob, T. A., Havlík, M. & Dolenský, B. In-flight epimerization of a bis-Tröger base. *Angewandte Chemie International Edition* **50**, 2401-2404 (2011).
40 Gotoh, H., Uchimaru, T. & Hayashi, Y. Two Reaction Mechanisms via Iminium Ion Intermediates: The Different Reactivities of Diphenylprolinol Silyl Ether and Trifluoromethyl-Substituted Diarylprolinol Silyl Ether. *Chemistry–A European Journal* **21**, 12337-12346 (2015).

41 Moberg, C. Mechanism of Diphenylprolinol Silyl Ether Catalyzed Michael Addition Revisited—but Still Controversial. *Angewandte Chemie International Edition* **52**, 2160-2162 (2013).
42 Gabelica, V. & Marklund, E. Fundamentals of ion mobility spectrometry. *Current opinion in chemical biology* **42**, 51-59 (2018).
43 Jensen, K. L., Dickmeiss, G., Jiang, H., Albrecht, Ł. & Jørgensen, K. A. The diarylprolinol silyl ether system: a general organocatalyst. *Accounts of chemical research* **45**, 248-264 (2012).
44 Zotova, N., Broadbelt, L. J., Armstrong, A. & Blackmond, D. G. Kinetic and mechanistic studies of proline-mediated direct intermolecular aldol reactions. *Bioorganic & medicinal chemistry letters* **19**, 3934-3937 (2009).
45 Zotova, N., Moran, A., Armstrong, A. & Blackmond, D. G. A Coherent Mechanistic Rationale for Additive Effects and Autoinductive Behaviour in Proline-Mediated Reactions. *Advanced Synthesis & Catalysis* **351**, 2765-2769 (2009).
46 Burés, J., Armstrong, A. & Blackmond, D. G. Curtin–Hammett paradigm for stereocontrol in organocatalysis by diarylprolinol ether catalysts. *Journal of the American Chemical Society* **134**, 6741-6750 (2012).
47 Bures, J., Armstrong, A. & Blackmond, D. G. Explaining anomalies in enamine catalysis:“downstream species” as a new paradigm for stereocontrol. *Accounts of chemical research* **49**, 214-222 (2016).
48 Schröder, D. Ion clustering in electrospray mass spectrometry of brine and other electrolyte solutions. *Physical Chemistry Chemical Physics* **14**, 6382-6390 (2012).
49 Jasǐková, L., Anania, M., Hybelbauerová, S. & Roithová, J. Reaction intermediates kinetics in solution investigated by electrospray ionization mass spectrometry: diaurated complexes. *Journal of the American Chemical Society* **137**, 13647-13657 (2015).
50 Schulz, J., Jašík, J., Gray, A. & Roithová, J. Formation of oxazoles from elusive gold (I) α-oxocarbenes: A mechanistic study. *Chem.-Eur. J* **22**, 9827-9834 (2016).
51 Jašík, J., Žabka, J., Roithová, J. & Gerlich, D. Infrared spectroscopy of trapped molecular dications below 4 K. *International Journal of Mass Spectrometry* **354**, 204-210 (2013).
52 Frisch, M. *et al.* (Gaussian, Inc. Wallingford, CT, 2016).
53 Ewing, S. A., Donor, M. T., Wilson, J. W. & Prell, J. S. Collidoscope: an improved tool for computing collisional cross-sections with the trajectory method. *Journal of The American Society for Mass Spectrometry* **28**, 587-596 (2017).